Electronic Supplementary Information

Experimental section

Materials: Sodium nitrate ($NaNO_3$, 99.0%), sodium nitrite ($NaNO_2$, 99.0%), ammonium chloride (NH_4Cl), sodium hydroxide (NaOH), sodium sulfite (Na_2SO_3), sodium salicylate ($C_7H_5NaO_3$), trisodium citrate dihydrate ($C_6H_5Na_3O_7 \cdot 2H_2O$), p-dimethylaminobenzaldehyde ($C_9H_{11}NO$), sodium nitroferricyanide dihydrate ($C_5FeN_6Na_2O \cdot 2H_2O$), 0.8 wt% sulfamic acid solution (H_3NO_3S), sodium hypochlorite solution (NaClO), sulfur powder (S), iron nitrate nonahydrate ($Fe(NO_3)_3 \cdot 9H_2O$), and iron sulfate heptahydrate ($FeSO_4 \cdot 7H_2O$) were purchased from Aladdin Ltd. (Shanghai, China). Sulfuric acid (H_2SO_4), hydrogen peroxide (H_2O_2), hydrochloric acid (HCl), hydrazine monohydrate ($N_2H_4 \cdot H_2O$), and ethylalcohol (C_2H_5OH) were bought from Beijing Chemical Corporation Ltd (Beijing, China). Titanium plate (TP) was purchased from Qingyuan Metal Materials Co., Ltd (Xingtai, China). All reagents used in this work were analytical grade without further purification.

Preparation of FeS_2@TiO_2/TP: FeS_2@TiO_2/TP was synthesized via a simple three-step procedure. Firstly, the well-cut small pieces (2.0 × 4.0 cm^2) titanium plates were sonicated in acetone, ethanol, and distilled water for 15 min, respectively. Then, the Teflon-lined autoclave contained the titanium plates immersing in 40 mL of 5 M NaOH aqueous solution and was put into an electric oven at 180 ℃ for 24 h. After cooling down to room temperature, the samples were moved out, washed with deionized water and ethanol several times, and dried at 60 ℃ for 30 min. Then the samples were

immersed in 0.25 M $Fe(NO_3)_3 \cdot 9H_2O$ for 1 h in order to exchange Na^+ with Fe^{3+}. The as-prepared Fe-titanate was rinsed with deionized water and ethanol several times. And then they were dried at 60 ℃ for 30 min. Subsequently, Fe-titanate was annealed in a tube furnace with S powder (0.2 g) at 500 °C under an argon atmosphere for 2 h. After cooling to room temperature, $FeS_2@TiO_2$/TP was finally obtained.

Preparation of TiO_2/TP and FeS_2: Pristine TiO_2/TP nanobelts array was synthesized using the same methods but with 1 M HCl for ion-exchange. The as-prepared $H_2Ti_2O_5 \cdot H_2O$ was then washed with DI water and ethanol several times and dried at 60 ℃ for 30 min. Subsequently, $H_2Ti_2O_5 \cdot H_2O$ was annealed in a tubular furnace at 500 ℃ under an argon atmosphere for 2 h. After cooling to room temperature, TiO_2/TP was finally obtained. 0.92 g of $FeSO_4$ and 3.2 g of Na_2SO_3 were mixed in 40 ml of DI water separately and added into a Teflon lined stainless steel autoclave which was maintained at 180 ℃ for 2 h. The FeS_2 was achieved after centrifugation and washing.

Characterizations: The crystal structure was confirmed by X-ray diffraction patterns obtained from a LabX XRD-6100 X-ray diffractometer (SHIMADZU, Japan) with a Cu Kα (40 kV, 30 mA) irradiation (λ= 0.154 nm). The observation of morphologies and composition were carried out on a GeminiSEM 300 scanning electron microscope (SEM) measurement (ZEISS Sigma 300) at an accelerating voltage of 5 kV equipped with energy dispersive X-ray (EDX). Transmission electron microscopy (TEM) images were collected by a Zeiss Libra 200FE transmission electron microscope operated at 200 kV. X-ray photoelectron spectroscopy (XPS) was performed on an ESCALABMK

II X-ray photoelectron spectrometer using Mg as the exciting source to investigate the surface chemical environment. The Ultraviolet-Visible (UV-Vis) absorbance data was measured by UV-visible Spectrophotometer. Gas chromatography (GC-2014C, SHIMADZU) was used for the quantitative detection of H_2 and N_2. ^1H NMR spectra were collected on Varian VNMRS 600 MHz (the USA).

Electrochemical measurements: All the electrochemical measurements were investigated in an H-shape reactor separated by a treated Nafion 117 membrane by using the CHI660E electrochemical workstation (Chenhua, Shanghai) with a standard three-electrode setup (FeS_2@TiO_2 (1 × 0.5 cm^2) as the working electrode, a Pt as the counter electrode, and a Hg/HgO as the reference electrode). The electrolyte solution was Ar-saturated 0.1 M NaOH with 0.1 M NO_3^-. All the potentials reported in our work were converted to reversible hydrogen electrode (RHE) scale via calibration with the following equation: E (RHE) = E (vs. Hg/HgO) + 0.0591 × pH + 0.098 V, and the current density was normalized by the geometric surface area.

Determination of NH_3: The concentration of produced NH_3 was determined by spectrophotometry measurement with the indophenol blue method.[1] The indophenol blue method is employed by the following Bethelot reaction queation.[2,3]

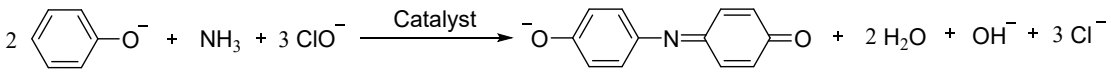

The ammonia reacts with phenol and hypochlorite in alkaline solution. The generated indophenol product is in blue color. The obtained electrolyte was firstly diluted 50 times

for further test. In detail, 2 mL of the diluted catholyte was obtained from the cathodic chamber and mixed with 2 mL of the 1 M NaOH solution that contained 5% salicylic acid and 5% sodium citrate. Then, 1 mL of 0.05 M NaClO and 0.2 mL of 1 wt% $C_5FeN_6Na_2O$ were dropped into the collected electrolyte solution. After standing at room temperature for 2 h, the ultraviolet-visible absorption spectrum was measured. The concentration-absorbance curve was calibrated using the standard NH_4Cl solution with NH_3 concentrations of 0.1, 0.25, 0.5, 1.5, 2.0, 3.0 and 4.0 μg mL^{-1} in 0.1 M NaOH. The absorbance at 655 nm was measured to quantify the NH_3 concentration using standard NH_4Cl solutions ($y = 0.4378x + 0.02455$, $R^2 = 0.9998$).

Determination of NO_2^-: The NO_2^- concentration was analyzed using the Griess test.[4] The Griess reagent was prepared by dissolving 0.1 g N-(1-naphthyl) ethylenediamine dihydrochloride, 1.0 g sulfonamide, and 2.94 mL H_3PO_4 in 50 mL deionized water. In a typical colorimetric assay, the 1.0 mL Griess reagent was mixed with the 1.0 mL nitrite-containing solution and 2.0 mL H_2O and allowed to react at room temperature for 10 mins, in which sulfonamide reacts with NO_2^- to form a diazonium salt and then further reacts with the amine to form an azo dye (magenta). The absorbance at 540 nm was measured to quantify the NO_2^- concentration with a standard curve of NO_2^- ($y = 2.0295x + 0.096$, $R^2 = 0.9998$).

Determination of N_2H_4: In this work, we used the method of Watt and Chrisp[5] to determine the concentration of produced N_2H_4. The chromogenic reagent was a mixed solution of 5.99 g $C_9H_{11}NO$, 30 mL HCl and 300 mL C_2H_5OH. In detail, 1 mL

electrolyte was added into 1 mL prepared color reagent and stirred for 15 min in the dark. The absorbance at 455 nm was measured to quantify the N_2H_4 concentration with a standard curve of hydrazine ($y = 0.6876x + 0.1068$, $R^2 = 0.9998$).

Determination of FE and NH_3 yield: FE toward NH_3 via NO_3RR is calculated by the following equation:

$$FE = (8 \times F \times [NH_3] \times V) / (M_{NH_3} \times Q) \times 100\%$$

NH_3 yield is calculated by the following equation:

$$NH_3 \text{ yield} = ([NH_3] \times V) / ((M_{NH_3} \times t \times A)$$

Where F is the Faradic constant (96485 C mol^{-1}), $[NH_3]$ is the measured NH_3 concentration, V is the volume of electrolyte in the anode compartment (80 mL), M_{NH_3} is the molar mass of NH_3, Q is the total quantity of applied electricity, t is the electrolysis time and A is the loaded area of catalyst (1×0.5 cm^2).

Computational details: Spin-polarized density functional theory (DFT) method was employed in all computations.[6,7] The core electrons were described using the projector-augmented-wave (PAW) method, while the Perdew–Burke–Ernzehof (PBE) functional with in the generalized gradient approximation (GGA) was utilized to treat the electronic exchange-correlation energy.[8] The spin polarization was adopted and its influence on the energy minima were also considered for all calculations.[9] All atomic structures were optimized until the energy and force reached the convergence thresholds of 10^{-4} eV and -0.02 eV/ Å, respectively. The energy cutoff was set to 450 eV. A Monkhorst-Pack k-mesh with a $4 \times 4 \times 1$ k-point grid was used for structural

optimization and frequency calculations, while 6 × 6 × 1 k-point grid was utilized for electronic structure calculations. The Gibbs free energy change (ΔG) involved in each elementary reaction calculation was calculated based on terms of the computational hydrogen electrode model proposed by Nørskov et al.[10,11] The calculation formula is: $\Delta G=\Delta E + \Delta ZPE - T\Delta S + eU + \Delta G_{pH}$. Here, ΔE is the DFT-calculated total energy, T is set to 298.15 K and the entropy S is computed by fixing the catalyst base as the premise. U is the electrode potential versus reversible hydrogen electrode (RHE). ΔG_{pH} represents the correction of the free energy because of the variations in pH conditions. ΔG_{max} represents the maximum ΔG among each elementary reaction.

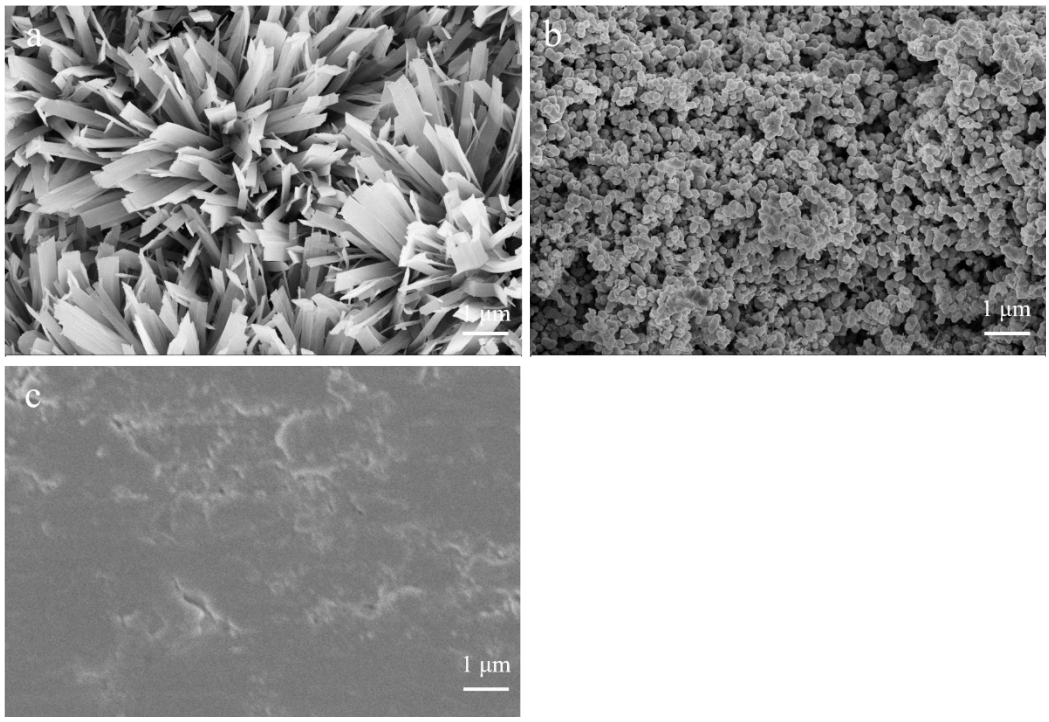

Fig. S1. SEM images of (a) TiO_2/TP, (b) FeS_2 nanoparticles, and (b) TP.

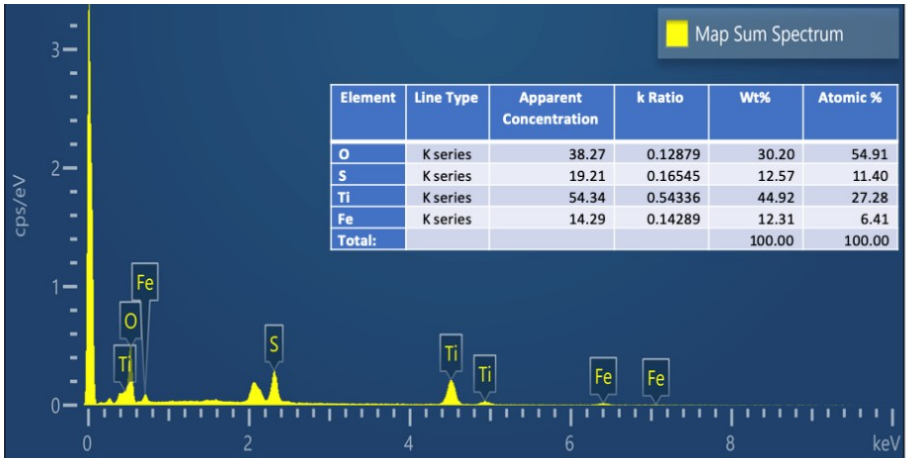

Element	Line Type	Apparent Concentration	k Ratio	Wt%	Atomic %
O	K series	38.27	0.12879	30.20	54.91
S	K series	19.21	0.16545	12.57	11.40
Ti	K series	54.34	0.54336	44.92	27.28
Fe	K series	14.29	0.14289	12.31	6.41
Total:				100.00	100.00

Fig. S2. Atomic ratios of the elements in FeS_2@TiO_2/TP.

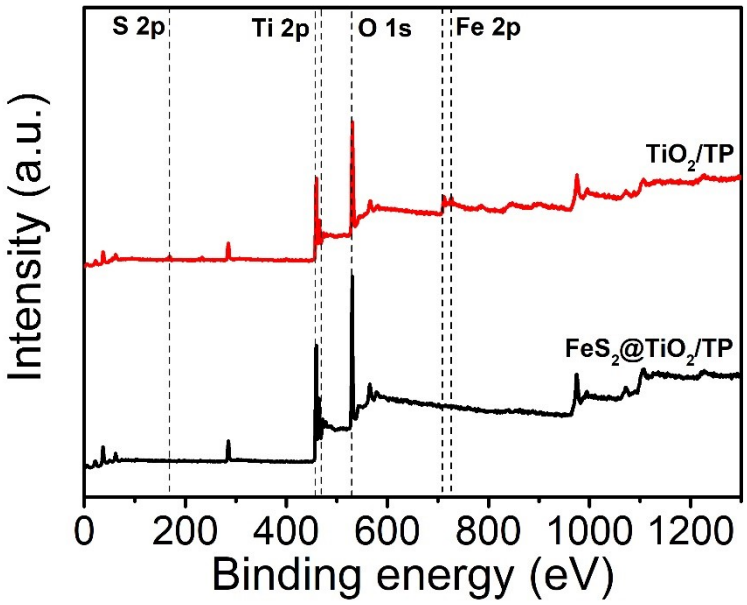

Fig. S3. XPS spectra of TiO_2/TP and FeS_2@TiO_2/TP.

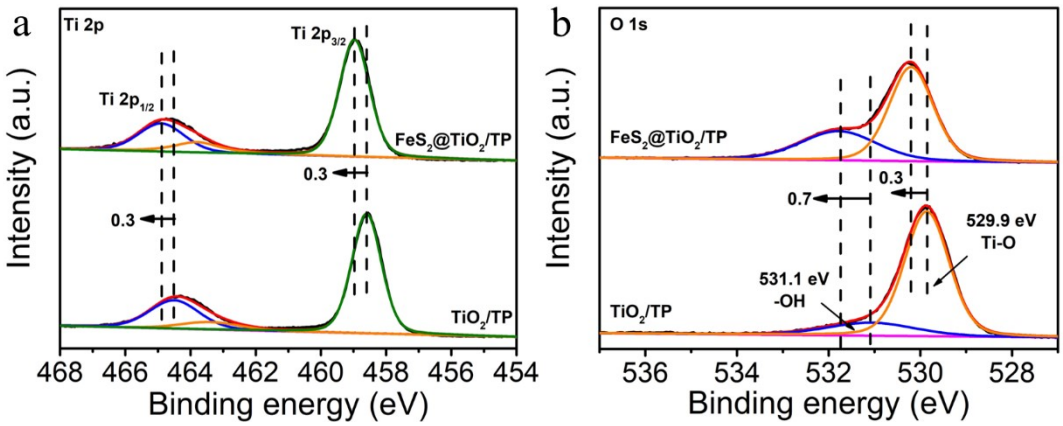

Fig. S4. XPS spectra of pristine TiO_2/TP and FeS_2@TiO_2/TP in the (a) Ti 2p and (b) O 1s.

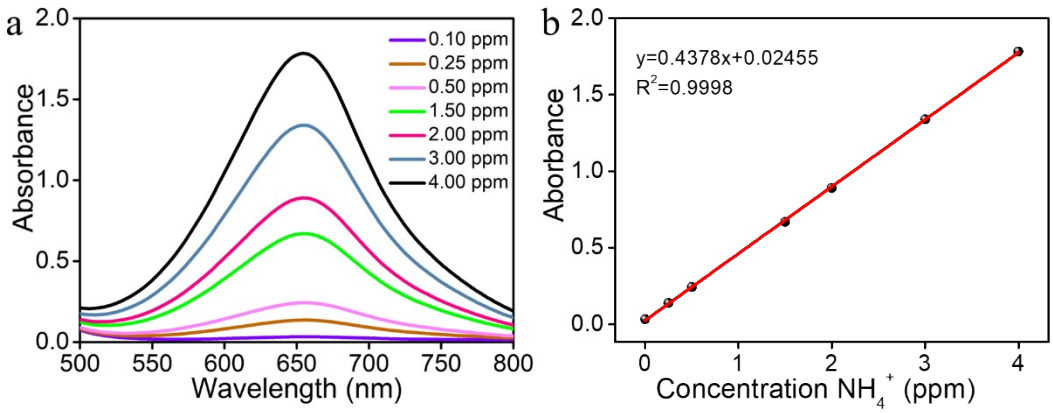

Fig. S5. (a) UV-Vis absorption spectra of indophenol assays kept with different concentrations of NH_4^+ after incubated for 2 h at room temperature. (b) Calibration curve used for estimation of NH_4^+ concentration.

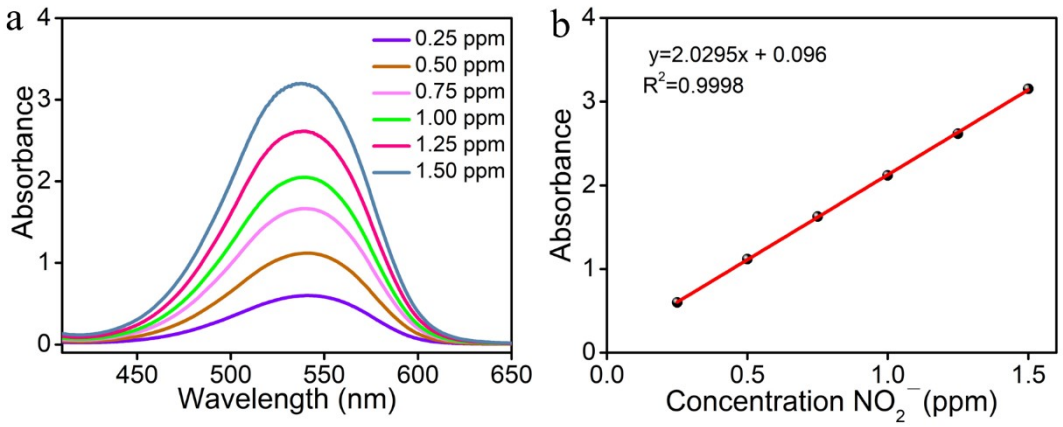

Fig. S6. UV-Vis absorption spectra of various NO_2^- concentrations after incubated for 10 mins at room temperature. (b) Calibration curve used for quantification of NO_2^- concentration.

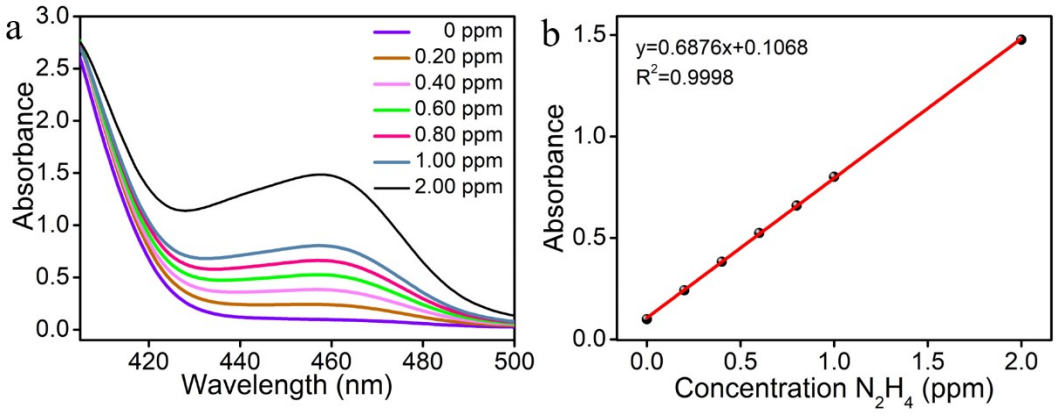

Fig. S7. (a) UV-Vis absorption spectra of various N_2H_4 concentrations after incubated for 15 mins at room temperature. (b) Calibration curve used for calculation of N_2H_4 concentration.

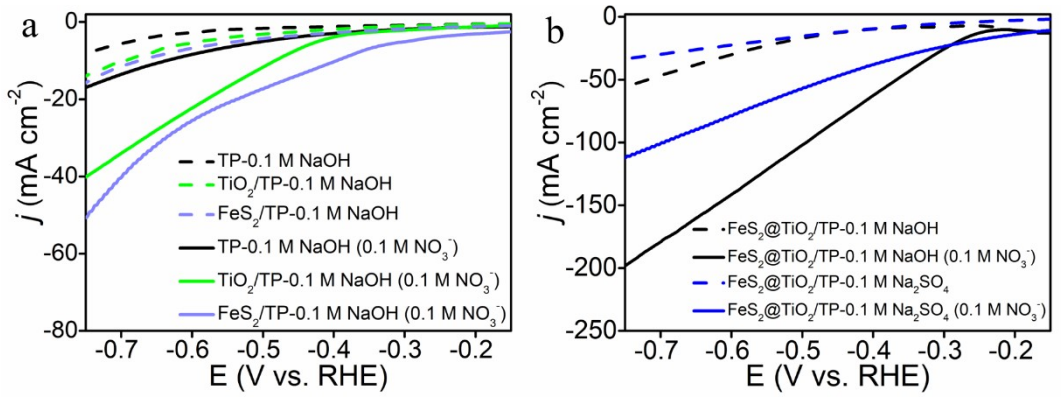

Fig. S8. (a) LSV curves of TP, TiO_2/TP and FeS_2/TP in 0.1 M NaOH with and without 0.1 M NO_3^-. (b) LSV curves of FeS_2@TiO_2/TP in alkaline and neutral electrolyte with and without 0.1 M NO_3^-.

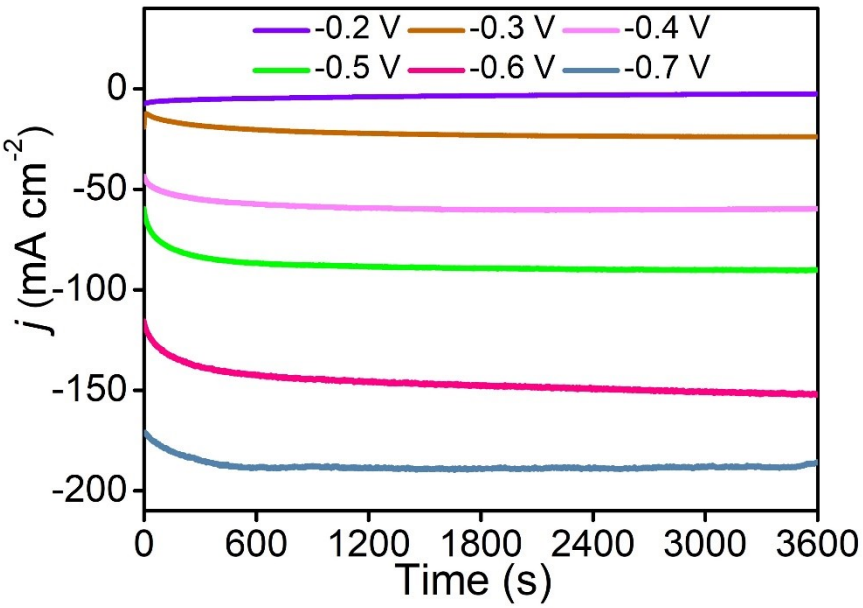

Fig. S9. Chronoamperometry curves of FeS_2@TiO_2/TP at different given potentials.

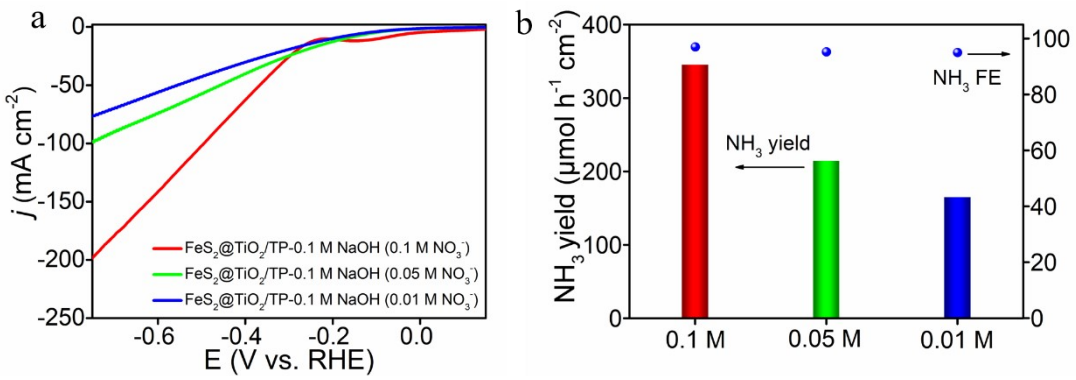

Fig. S10. (a) LSV curves and (b) NH_3 yields and FEs in 0.1 M NaOH with different NO_3^- concentrations.

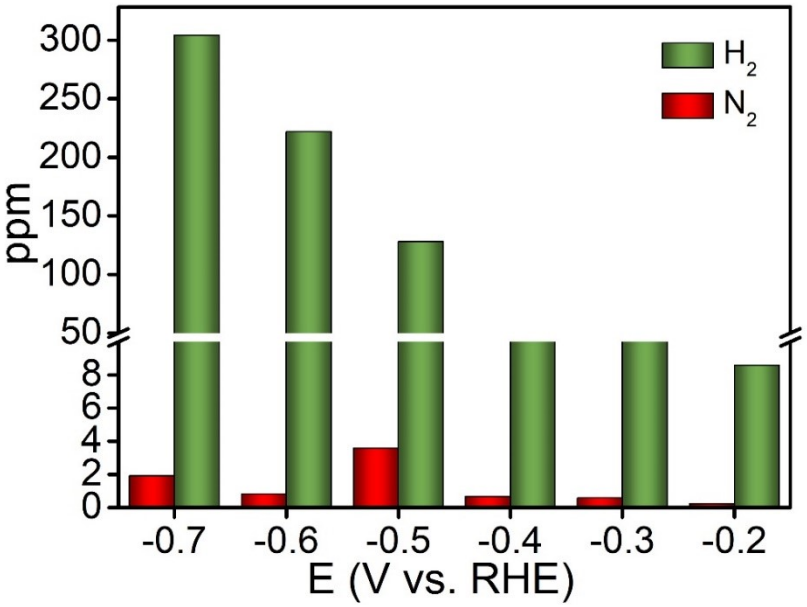

Fig. S11. The concentrations of gas byproducts H_2 and N_2 detected by gas chromatography.

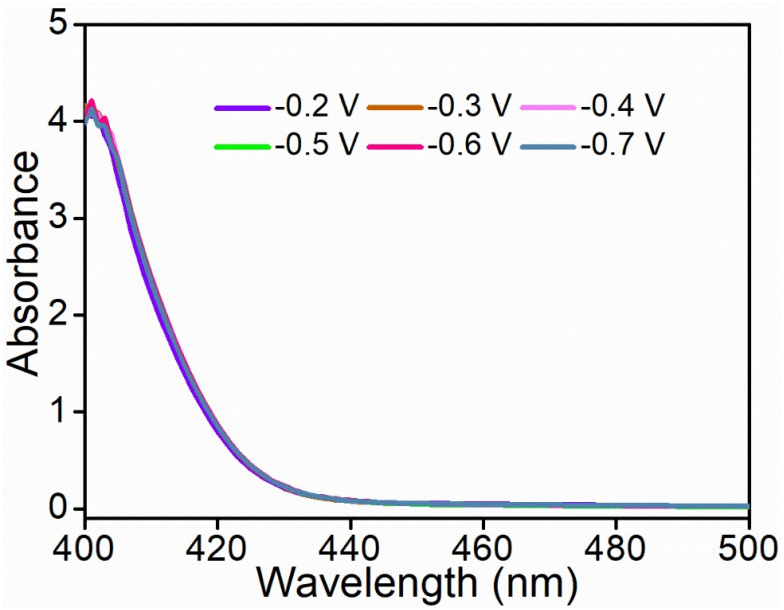

Fig. S12. UV-Vis absorption spectra of produced N_2H_4.

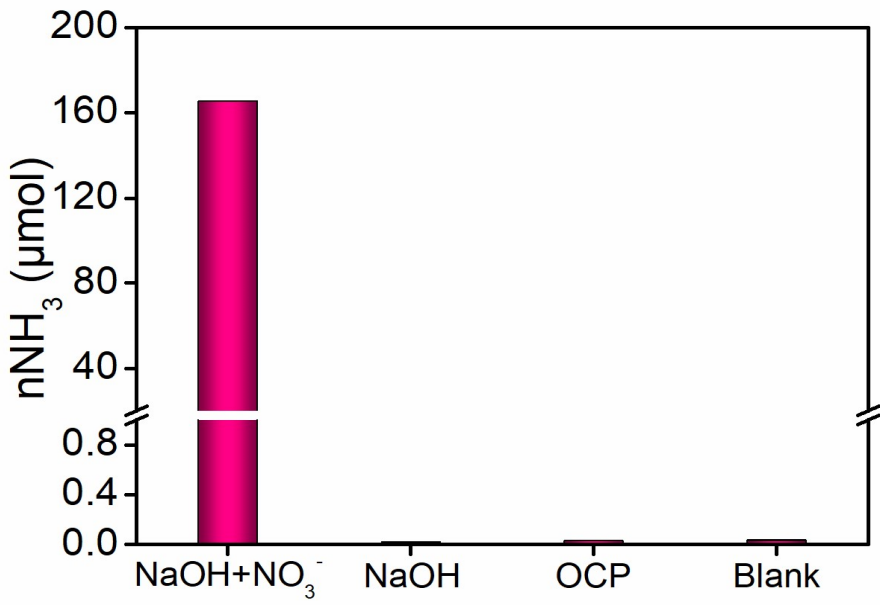

Fig. S13. Comparison of the amount of produced NH_3 under four different conditions.

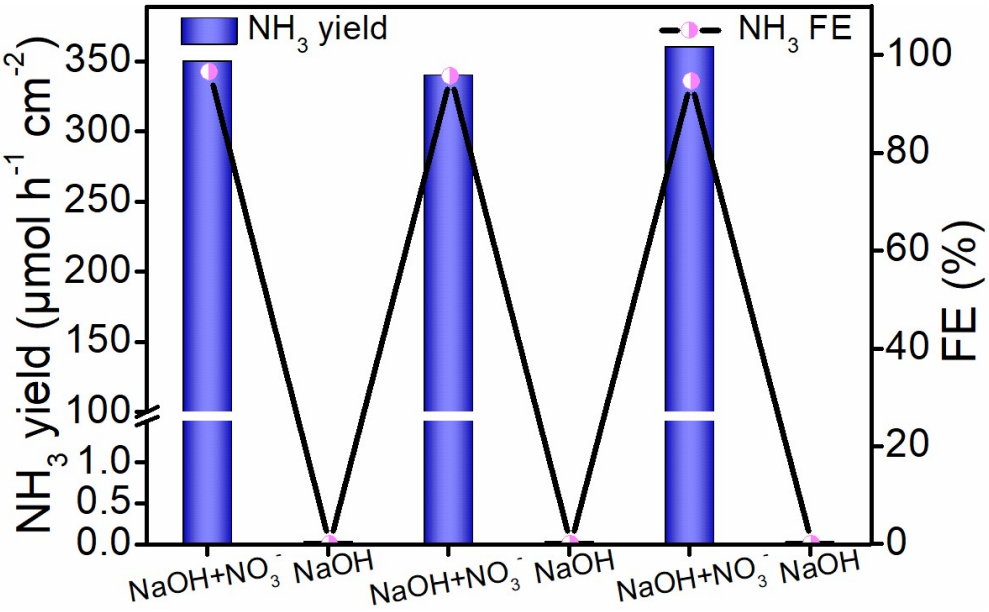

Fig. S14. NH_3 yields and FEs of FeS_2@TiO_2/TP during the alternating cycling test between 0.1 M NaOH with and without additional 0.1 M NO_3^-.

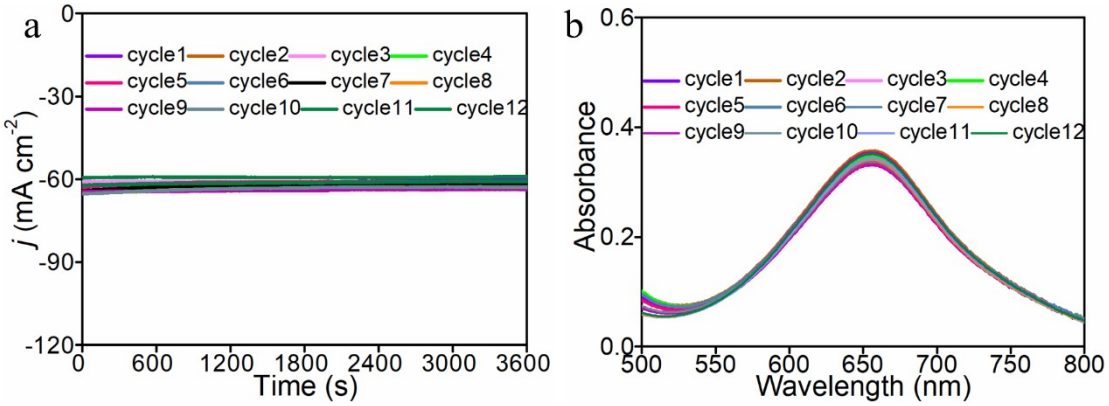

Fig. S15. (a) Chronoamperometry curves and (b) corresponding UV-Vis absorption spectra of FeS_2@TiO_2/TP for electrogenerated NH_3 during cycling tests at -0.4 V.

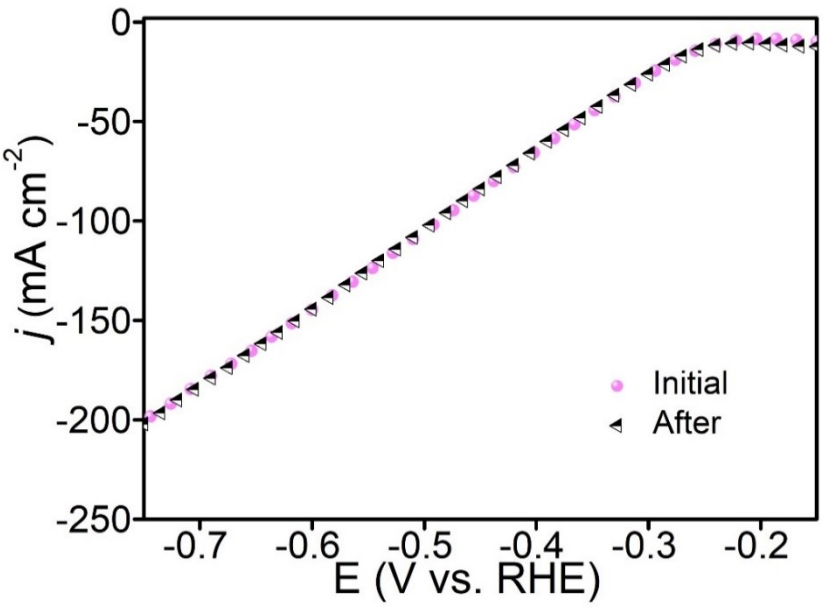

Fig. S16. LSV curves of FeS_2@TiO_2/TP before and after 24-h electrolysis.

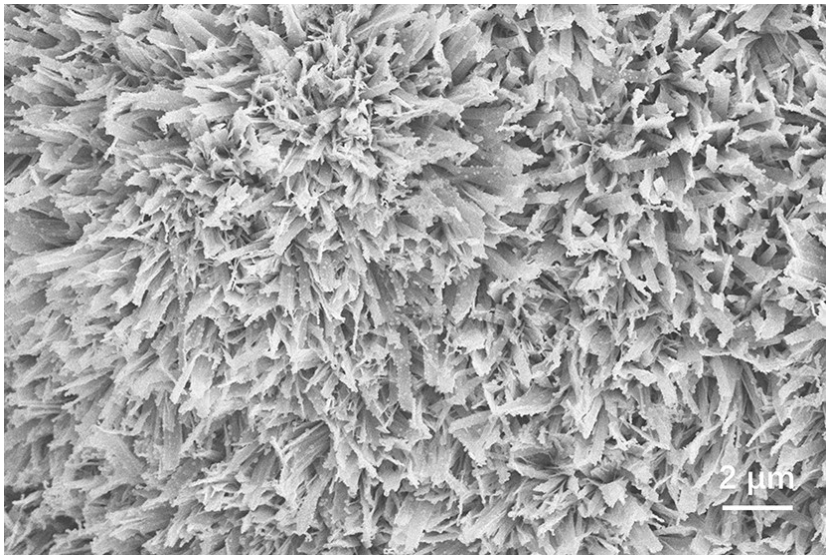

Fig. S17. SEM image of FeS_2@TiO_2/TP after 24-h electrolysis.

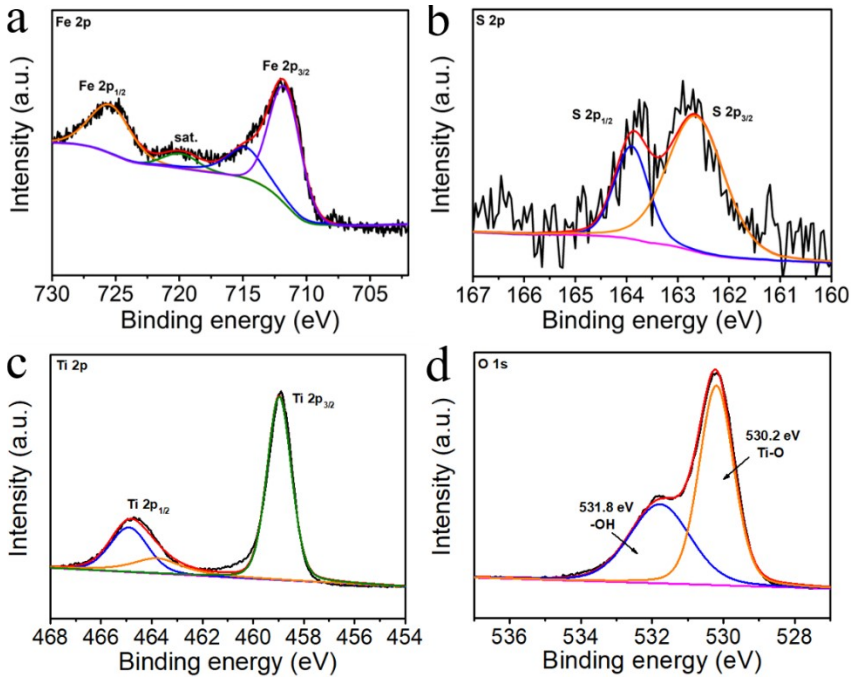

Fig. S18. (a) XPS spectra of post-test FeS_2@TiO_2/TP: (a) Fe 2p, (b) S 2p, (c) Ti 2p, and (d) O 1s.

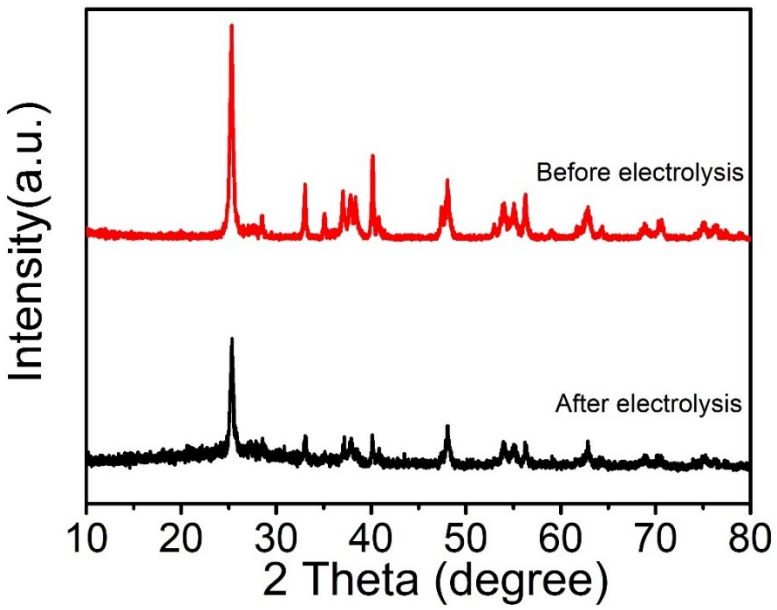

Fig. S19. XRD patterns of FeS_2@TiO_2/TP before and after 24-h electrolysis.

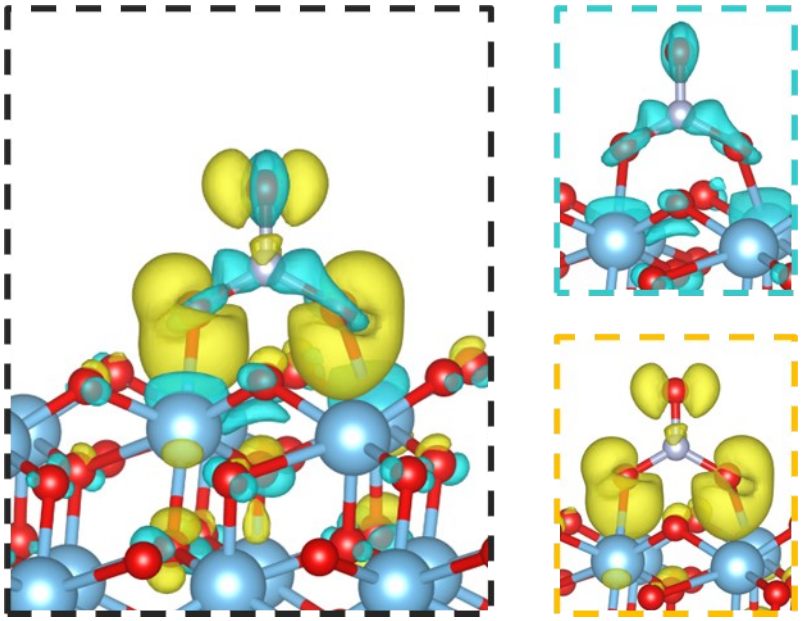

Fig. S20. Charge density difference of TiO_2 with adsorbed NO_3^-, where yellow and cyan color indicate electron accumulation and depletion, respectively. The isosurface value was set to 0.000194Å^{-3}.

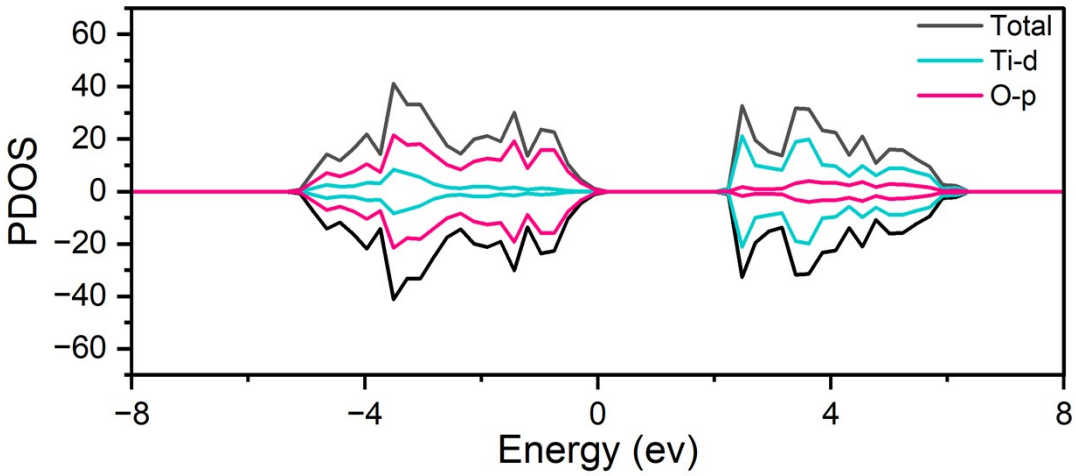

Fig. S21. Partial density of states (PDOS) of TiO_2.

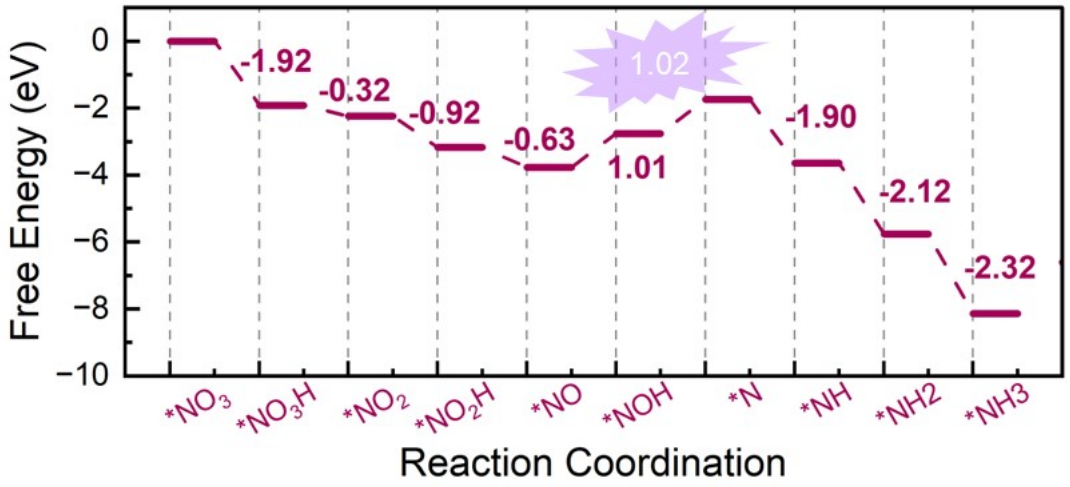

Fig. S22. Gibbs free energy diagrams for NO_3RR on TiO_2.

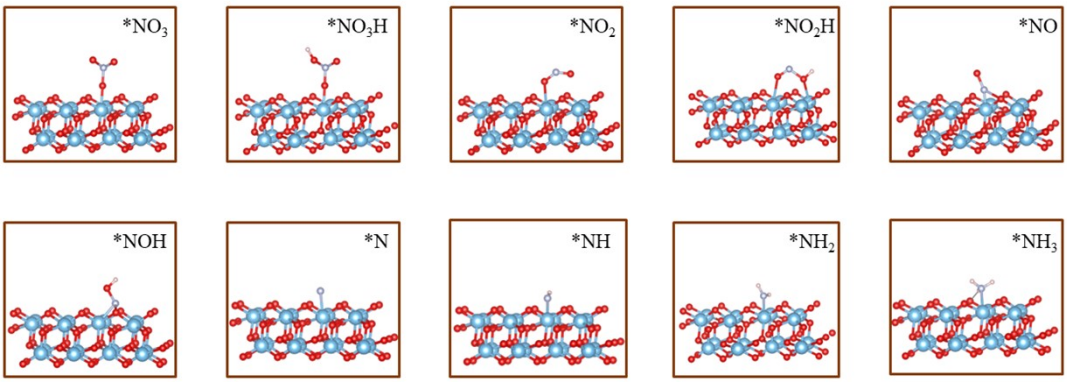

Fig. S23. Configuration transformation of intermediates during NO_3RR on TiO_2.

Table S1. Comparison of catalytic performance of FeS_2@TiO_2/TP with other reported NO_3RR electrocatalysts.

Catalyst	Electrolyte	NH_3 yield@Potential (V vs. RHE)	FE@Potential (V vs. RHE)	Ref.
FeS_2@TiO_2/TP	0.1 M NaOH (0.1 M NO_3^-)	860.3 μmol h^{-1} cm^{-2}@-0.7	97.0%@-0.4	This work
Cu clusters/TiO_{2-x}	0.5 M Na_2SO_4 (200 ppm NO_3^-	0.1143 mmol h^{-1} mg^{-1}@-0.75	81.34%@-0.75	12
TiO_{2-x}	0.5 M Na_2SO_4 (50 ppm NO_3^-)	0.045 mmol h^{-1} mg^{-1}@-0.95	85.0%@-0.95	13
Cu/TNTA	0.1 M Na_2SO_4 (50 mgN/L NO_3^-)		84.3%@-0.65 (NO_3^- removal efficiency)	14
Ni NP	1 M NaOH (20 mM NO_3^-)	/	46.3%@-0.27	15
Fe SAC	1 M KOH (0.1 M NO_3^-)	/	86%@-0.21	16
Cu	1 M NaOH (0.1 M NO_3^-)	/	79%	17
$Cu_{50}Ni_{50}$	1 M KOH (10 mM NO_3^-)	/	84 ± 2%	18
Pd facets	0.1 M NaOH (20 mM NO_3^-)	18 μmol h^{-1} cm^{-2}@-0.2	35%@-0.2	19
In-S-G	1 M KOH (0.1 M NO_3^-)	22 μmol h^{-1} $mg_{cat.}^{-1}$@-0.5	75%@-0.5	20
Pd/TiO_2	0.5 M NaOH (0.25 M NO_3^-)	66 μmol h^{-1} cm^{-2}@-0.7	92%@-0.7	21
BC_2N/Pd	0.1 M KOH (0.25 M NO_3^-)	100 μmol h^{-1} cm^{-2}@-0.7	97.42%@-0.3	22
Fe-PPy SACs	0.1 M KOH (0.1 M NO_3^-)	160 μmol h^{-1} cm^{-2}@-0.7	~100%@-0.3	23
BCN@Ni	0.1 M KOH (0.1 M NO_3^-)	140 μmol h^{-1} cm^{-2}@-0.5	91.15%@-0.3	24
Ni_3B@$NiB_{2.74}$	0.1 M KOH (0.1 M NO_3^-)	200 μmol h^{-1} cm^{-2}@-0.3	~100%@-0.3	25

BCN-Cu	0.1 M KOH (100 mM NO_3^-)	110 μmol h^{-1} cm^{-2}@-0.5	98.23@-0.5	26
$ZnCo_2O_4$	0.1 M KOH (0.1 M NO_3^-)	120 μmol h^{-1} $mg_{cat.}^{-1}$@-0.6	95.4%@-0.4	27
Co/CoO NSA	0.1 M K_2SO_4 (200 ppm NO_3^-)	200 μmol h^{-1} cm^{-2}@-0.65	93.8%@-0.65	28

References

1 D. Zhu, L. Zhang, R. E. Ruther and R. J. Hamers, *Nat. Mater.*, 2013, **12**, 836-841.

2 Y. Zhao, R. Shi, X. Bian, C. Zhou, Y. Zhao, S. Zhang, F. Wu, G. I. N. Waterhouse, L. Z. Wu, C. H. Tung and T. Zhang, *Adv. Sci.*, 2019, **6**, 1802109.

3 D. Yao, C. Tang, L. Li, B. Xia, A. Vasileff, H. Jin, Y. Zhang and S. Z. Qiao, *Adv. Energy Mater.*, 2020, **10**, 2001289.

4 G. W. Watt and J. D. Chrisp, *Anal. Chem.*, 1952, **24**, 2006-2008.

5 G. Kresse and J. Hafner, *Phys. Rev. B*, 1994, **49**, 14251-14269.

6 Q. Zhou, F. Gong, Y. Xie and R. Xiao, *Green Energy Environ.*, 2022, https://doi.org/10.1016/j.gee.2022.06.005.

7 Q. Zhou, F. Gong, Y. Xie, D. Xia, Z. Hu, S. Wang, L. Liu and R. Xiao, *Fuel*, 2022, **310**, 122442.

8 B. Wang, T. Li, F. Gong, M. H. D. Othman and R. Xiao, *Fuel Process. Technol.*, 2022, **235**, 107380.

9 X. Sun, F. Gong, M. Hao, L. Wu, C. Yin, Z. Sun and R. Xiao, *Appl. Surf. Sci.*, 2022, **582**, 152484.

10 Y. Qiu, E. Fu, F. Gong and R. Xiao, *Int. J. Hydrogen Energ.*, 2022, **47**, 5044-5052.

11 J. Chen, Q. Zhou, L. Yue, D. Zhao, L. Zhang, Y. Luo, Q. Liu, N. Li, A. A. Alshehri, M. S. Hamdy, F. Gong and X. Sun, *Chem. Commun.*, 2022, **58**, 3787-3790.

12 X. Zhang, C. Wang, Y. Guo, B. Zhang, Y. Wang and Y. Yu, *J. Mater. Chem. A.*, 2022, **10**, 6448-6453.

13 R. Jia, Y. Wang, C. Wang, Y. Ling, Y. Yu and B. Zhang, *ACS Catal.*, 2022, **10**, 3533-3540.

14 Q. Song, S. Zhang, X. Hou, J. Li, L. Yang, X. Liu and M. Li, *J. Hazard. Mater.*, 2022, **438**, 129455.

15 L. Mattarozzi, S. Cattarin, N. Comisso, P. Guerriero, M. Musiani, L. Vázquez-Gómez and E. Verlato, *Electrochim. Acta*, 2013, **89**, 488-496.

16 Z. Wu, M. Karamad, X. Yong, Q. Huang, D. A. Cullen, P. Zhu, C. Xia, Q. Xiao, M. Shakouri, F. Chen, J. Y. Kim, Y. Xia, K. Heck, Y. Hu, M. S. Wong, Q. Li, I.

Gates, S. Siahrostami and H. Wang, *Nat. Commun.*, 2021, **12**, 2870.

17 D. Reyter, G. Chamoulaud, D. Bélanger and L. Roué, *J. Electroanal. Chem.*, 2006, **596**, 13-24.

18 Y. Wang, A. Xu, Z. Wang, L. Huang, J. Li, F. Li, J. Wicks, M. Luo, D. H. Nam, C. Tan, Y. Ding, J. Wu, Y. Lum, C. T. Dinh, D. Sinton, G. Zheng and E. H. Sargent, *J. Am. Chem. Soc.*, 2020, **142**, 5702-5708.

19 J. Lim, C. Liu, J. Park, Y. Liu, T. P. Senftle, S. W. Lee and M. C. Hatzell, *ACS Catal.*, 2021, **11**, 7568-7577.

20 F. Lei, W. Xu, J. Yu, K. Li, J. Xie, P. Hao, G. Cui and B. Tang, *Chem. Eng. J.*, 2021, **426**, 131317.

21 Y. Guo, R. Zhang, S. Zhang, Y. Zhao, Q. Yang, Z. Huang, B. Dong and C. Zhi, *Energy Environ. Sci.*, 2021, **14**, 3938-3944.

22 X. Li, X. Zhao, Y. Zhou, J. Hu, H. Zhang, X. Hu and G. Hu, *Appl. Surf. Sci.*, 2022, **584**, 152556.

23 P. Li, Z. Jin, Z. Fang and G. Yu, *Energy Environ. Sci.*, 2021, **14**, 3522-3531.

24 X. Zhao, Z. Zhu, Y. He, H. Zhang, X. Zhou, W. Hu, M. Li, S. Zhang, Y. Dong, X. Hu, A. V. Kuklin, G. V. Baryshnikov, H. Ågren, T. Wågberg and G. Hu, *Chem. Eng. J.*, 2022, **433**, 133190.

25 L. Li, C. Tang, X. Cui, Y. Zheng, X. Wang, H. Xu, S. Zhang, T. Shao, K. Davey and S. Qiao, *Angew. Chem. Int. Ed.*, 2021, **60**, 14131-14137.

26 X. Zhao, X. Jia, Y. He, H. Zhang, X. Zhou, H. Zhang, S. Zhang, Y. Dong, X. Hu, A. V. Kuklin, G. V. Baryshnikov, H. Ågren and G. Hu, *Appl. Mater. Today*, 2021, **25**, 101206.

27 P. Huang, T. Fan, X. Ma, J. Zhang, Z. Chen and X. Yi, *ChemSusChem*, 2022, **15**, e202102049.

28 Y. Yu, C. Wang, Y. Yu, Y. Wang and B. Zhang, *Sci. China Chem*, 2020, **63**, 1469-1476.